

# Dark Matter Simulations with Primordial Black Holes in the Early Universe

Maxim V. Tkachev<sup>1\*</sup> Sergey V. Pilipenko<sup>1†</sup>, and Gustavo Yepes<sup>2,3</sup>

<sup>1</sup>*Astro Space Center, P. N. Lebedev Physical Institute of RAS, Profsojuznaya 84/32, Moscow 117997, Russia*

<sup>2</sup>*Departamento de Física Teórica, Módulo 8 Universidad Autónoma de Madrid, 28049 Madrid, Spain*

<sup>3</sup>*Centro de Investigación Avanzada en Física Fundamental (CIAFF), Universidad Autónoma de Madrid, 28049 Madrid, Spain*

Accepted XXX. Received YYY; in original form ZZZ

## ABSTRACT

Primordial Black Holes (PBH) with masses of order  $10 - 30M_{\odot}$  have been proposed as a possible explanation of the gravitational waves emission events recently discovered by the LIGO observatory. If true, then PBHs would constitute a sizeable fraction of the dark matter component in the Universe. Using a series of cosmological N-body simulations which include both dark matter and a variable fraction of PBHs ranging from  $f_{PBH} = 10^{-4}$  to  $f_{PBH} = 1$ , we analyse the processes of formation and disruption of gravitationally bound PBH pairs, as well as the merging of both bound and unbound pairs, and estimate the probabilities of such events. We show that they are in good agreement with the constraints to the PBH abundance obtained by the LIGO and other research groups. We find that pair stability, while being a main factor responsible for the merger rate, is significantly affected by the effects of dark matter halo formation and clustering. As a side result, we also evaluate the effects of numerical errors in the stability of bound pairs, which can be useful for future research using this methodology.

**Key words:** cosmology-simulations — dark matter — primordial black holes

## 1 INTRODUCTION

Various astrophysical and cosmological observations provide substantial evidences that firmly establish the existence of a dominated collisionless, non-baryonic, dark matter (DM) component in our Universe. However, the nature of DM remains one of the major unsolved problems in fundamental physics.

Primordial black holes (PBHs), originally proposed for the first time by Zel'dovich & Novikov (1966), can be formed during the early stages of the evolution of the Universe due to the collapse of large energy density fluctuations. They have been proposed as promising candidates for DM (Lacki & Beacom 2010; Clesse & García-Bellido 2017; Kashlinsky 2016; Espinosa et al. 2018; Clesse & García-Bellido 2018). PBHs have recently received quite a lot of attention in relation to the events observed by The Advanced Laser Interferometer

Gravitational-Wave Observatory (LIGO) (Abbott et al. 2016a,b,c, 2017a,b,c)<sup>1</sup>.

Although, at present, the hypothesis of PBH existence is yet neither proven nor refuted, the very observational limits on its abundance represent themselves a powerful and unique method of investigating the early Universe at small scales, which cannot be tested by any other method (Carr et al. 2016, 2017; Sasaki et al. 2018). The most important potential bounds on the PBH abundance in the mass range around  $10 - 30 M_{\odot}$  can be obtained from LIGO observations, assuming, that they involve the merging of primordial black holes pairs. Despite the fact, that some of the LIGO events (The LIGO Scientific Collaboration et al. 2018) are now accepted as having astrophysical origin (Nitz et al. 2019) there still remain certain problems related with the formation of black holes of such masses originated from stellar evolution processes (see, e.g., Dolgov (2017)). Therefore, their origin could seem to be primordial. If PBHs made up a significant fraction of DM, the PBH merger rate would produce a gravitational wave (GW) background which would

\* mtkachev@asc.rssi.ru (MVT)

† spilipenko@asc.rssi.ru (SVP)

<sup>1</sup> LIGO/Virgo Public Alerts from the O3/2019 observational run can be found at <https://gracedb.ligo.org/superevents/public/O3/>

be much larger than what is currently observed by LIGO (Wang et al. 2016; Raidal et al. 2017; Ali-Haïmoud 2018), as well as other effects, such as gravitational lensing of supernovae (Zumalacárregui & Seljak 2018). However, SN lensing constraints were reanalysed by Garcia-Bellido et al. (2017) and showed to agree with observations. Likewise, LIGO constraints are also subject of large theoretical uncertainties.

A reliable estimate of the GW signatures from PBH binary mergers requires a good understanding of the process of formation of PBH binaries and their subsequent interactions with the surrounding matter that may disrupt the binaries (for example, see Raidal et al. (2019) or Trashorras et al. (2020)). Despite the fact that the bulk of this work is dedicated to PBH binaries, we also consider the effects of hyperbolic<sup>2</sup> close encounters (as suggested by García-Bellido & Nesseris (2017)), and how a proper account of these events could affect our final results.

In this paper we present a numerical model describing the evolution of PBHs with masses  $\sim 30 M_{\odot}$  throughout the earliest stages of the Universe and up to redshifts  $z \approx 3.0$ . Despite the aforementioned constraints on the abundance of PBHs of such masses, in our model, just for testing purposes, we also assume the extreme case where all of the DM consists of PBHs, i.e.,  $f_{PBH} = \frac{\Omega_{PBH,0}}{\Omega_{m,0}} = 1.0$ , where  $\Omega_{PBH,0}$  is the density parameter of PBHs at redshift  $z = 0$ , and  $\Omega_{m,0}$  is the total matter density parameter at the same redshift. However, our main conclusions are obtained from simulations with much smaller fractions, down to  $f_{PBH} = 10^{-4}$ .

We run a series of dark-matter only cosmological N-body simulation, using a modified version of the TREEPM cosmological code GADGET-2. To our knowledge, previous to our work, cosmological N-body codes have been applied for studying PBH problems only by Inman & Ali-Haïmoud (2019). Although, they pursued different goals, such as the detailed and wide-scale study of the interaction of "normal" and "PBH dark matter", while, as the authors themselves mentioned in that paper, "their numerical setup does not have high enough spatial resolution to resolve individual binary orbits". In our work, on the other hand, when  $f_{PBH} < 1.0$  we split the DM fluid into "PBH dark matter" represented as individual particles and a "normal dark matter", that is represented as a unperturbed, uniform medium. We then study the complex processes of formation, disruption and merging of PBH pairs from the orbits of the PBH particles in the context of a 2-body problem, where one body is a given PBH particle and the second body is one of its neighbours with the minimal total energy  $E$ . The total energy is computed as a product of specific orbital energy  $\epsilon$  and reduced mass  $\mu = \frac{m_1 m_2}{m_1 + m_2}$ , where  $m_1 = m_2 = M$  is a mass of a PBH:

$$E = \mu\epsilon = \frac{M}{2} \left( \frac{v^2}{2} - \frac{2GM}{r} \right), \quad (1)$$

where  $v$  is a relative velocities of the particles (including the Hubble velocity),  $r$  is the radius vector in physical coordinates. We evaluate the stability of a pair in general and its dependence on the numerical errors associated to gravitational softening parameter and timestep (see Section 3).

<sup>2</sup> In this context, "pair" is not necessarily a *gravitationally bound* pair, unless specifically mentioned, and in general should be perceived simply as "two interacting particles".

Additionally, as mentioned above, we also consider the possibility of binary capture due to the general relativity (GR) effects from close hyperbolic encounters. The merging process of both bound and unbound pairs is evaluated by estimating their rate of energy loss due to the radiation of gravitational waves. The merging condition is defined as

$$\sum_{i=1}^n T |\dot{E}| \geq \frac{GM^2}{2|a|} \quad (2)$$

where  $\dot{E}$  is the rate of energy loss by the pair due to the radiation of gravitational waves,  $T$  is the current orbital period of the pair, and  $a$  is a semi-major axis of the pair ( $a < 0$  for hyperbolic orbit). Since the majority of our pairs have eccentricities close to  $e \approx 1$ , we are safe to assume that a pair radiates gravitational waves only when its particles pass the pericentre. Therefore, the sum is limited to the number of full periods,  $n$ , during which a pair remained gravitationally bound, or 1 in case of hyperbolic orbit. The energy loss can be estimated as

$$\dot{E} = \frac{64G^4 M^5}{5c^5 a^5} g(e) \quad (3)$$

with

$$g(e) = \begin{cases} \frac{24 \cos^{-1}(-\frac{1}{e})(1 + \frac{73}{24}e^2 + \frac{37}{96}e^4) + (e^2 - 1)^{1/2}(\frac{301}{6} + \frac{673}{12}e^2)}{(e^2 - 1)^{7/2}}, & e \geq 1, \\ \frac{24\pi}{(1 - e^2)^{7/2}} (1 + \frac{73}{24}e^2 + \frac{37}{96}e^4), & e < 1, \end{cases} \quad (4)$$

and  $e$  being the eccentricity of the pair,  $G$  is the gravitational constant, and  $c$  is the speed of light in vacuum, respectively (Peters & Mathews 1963; Turner 1977). Both  $E$  and  $\dot{E}$  are calculated with orbital parameters that the pair has at a given moment. If the accumulated radiated energy of a given pair gets larger than  $E$ , and the pair is not disrupted during this time, the pair is considered to be merged. For an accurate description of the algorithm see Section 4.

The paper is organised as follows:

(i) In Section 2 we describe the details of our numerical model and provide the list of parameters used to run the N-body simulations.

(ii) In Section 3 we calculate the probabilities of the formation of PBH pairs, starting during the radiation dominated epoch. Then, we evaluate the possibilities for the pair to be disrupted due to numerical errors rather than to physical processes.

(iii) In Section 4 we provide our estimates of the merger rate of PBH pairs, depending on the fractional abundance of PBH, including hyperbolic captures due to GR effects.

(iv) Finally, we leave Section 5 for discussion regarding the question whether or not PBHs with masses of order of tens of solar masses can constitute a large enough fraction of dark matter to explain gravitational waves events as merging of PBHs.

## 2 N-BODY SIMULATIONS WITH PRIMORDIAL BLACK HOLES

We are mainly interested in finding and analysing the behaviour of PBH *pairs*. Therefore, their orbits should be cal-

culated with sufficient precision. Normally this would require the use of direct N-body methods, which are computationally very expensive for large number of particles. We use instead the publicly available N-body code **GADGET-2**<sup>3</sup> (Springel 2005), which is widely used for cosmological simulations. This code uses a combined Tree + Particle Mesh (TreeMP) algorithm to estimate the gravitational accelerations for each particle by decomposing the gravitational forces into a long range term, computed from Particle-Mesh methods, and short scale interactions from nearest neighbours using Tree methods. The code is MPI parallel and can be used with periodic boundary conditions in the co-moving frame. The scaling of the code with the number of particles is  $\mathcal{O}(N \log N)$  so it can handle a large number of particles with reasonable computational resources.

The simulations were run in the **MareNostrum** supercomputer at BSC-CNS<sup>4</sup> using a modified version of **GADGET-2** in which the free parameters of the code were chosen such that the force computation was accurate enough for PBH binaries to form and survive without being disrupted by pure numerical errors. We took the gravitational softening length  $\epsilon = 0.001$  pc and a timestep of  $\Delta t = 10^{-6}$  in  $\log(a)$ .

These parameters have a significant impact in the orbit stability, so we ensured that our choices are optimal and that a further reduction of both  $\epsilon$  and  $\Delta t$  does not yield any significant improvement in orbit stability.

Previous analytic estimates suggest that the first PBH pairs begin to appear approximately at the radiation-matter energy equipartition epoch ( $z \sim 10^3$ ) (Nakamura et al. 1997; Sasaki et al. 2016) or, depending on the PBH fraction, even earlier – during the radiation dominated epoch. Therefore, we had to modify the cosmological equations in the **GADGET-2** code to be valid during the radiation dominated epoch of the Universe, since we start our simulations at  $z_{init} = 10^5$ .

As was discussed earlier, in this work we focus on the formation of PBH pairs for different fractions of PBH to the total DM component. So, when  $f_{PBH} < 1.0$ , we have to split the DM into two types: "PBH DM" and "normal DM" (see Sec. 1).

As it is shown in Sec. 3, in our simulations virialised structures start to form as early as  $z \approx 10^3$ , which could be caused by the initial Poisson distribution of PBHs. This differs significantly from the case of standard  $\Lambda$ CDM model, where the first virialised structures start to form at  $z \simeq 40$ . Therefore we assume that the "normal DM" behaves as an uniform medium in our simulations. Nevertheless, we will discuss later why the formation of virialised structures is important and how it affects the behaviour of PBH pairs (see Sec. 3.3).

In order to quantify the range of redshifts in which this approximation is applicable, we calculate the fraction of virialised normal DM using the analytical Press-Schechter formalism for halos more massive than  $30 M_\odot$  (see Press & Schechter (1974)). We find that the fraction of virialised structures made of normal DM is less than 50% at  $z > 10$ . (see Figure 1).

Thus, the presence of normal DM influences the evolution of PBH DM only through its contribution to the com-

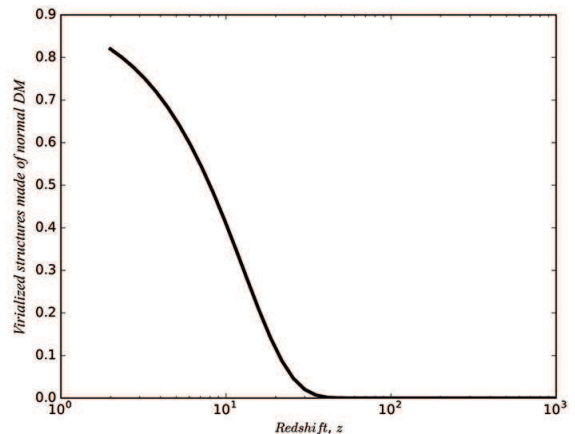


**Figure 1.** The fraction of virialised structures made of normal DM for halos more massive than  $30 M_\odot$ , as a function of redshift  $z$

putation of the Hubble function in the **GADGET-2** code:

$$H(z) = H_0 [\Omega_{\Lambda,0} + \Omega_{m,0}(1+z)^3 - \Omega_{r,0}(1+z)^4]^{\frac{1}{2}}, \quad (5)$$

For our purposes, this approach seems reasonable in terms of required accuracy and reasonable computational resources since we avoid the costly calculations of the interactions between DM and PBH particles.

We have run a series of six dark matter only simulations. Five of them correspond to different values of the PBH fraction, ranging from  $f_{PBH} = 1.0$  to  $f_{PBH} = 10^{-4}$ . For convergence study, we have also run an additional simulation with the PBH fraction  $f_{PBH} = 10^{-4}$  but increasing the number of particles. In all our simulations the PBH fraction is represented by up to  $N_{total} = 10^5$  particles with masses  $30 M_\odot$ . The initial conditions for PBH particles were set at  $z = 10^5$ . Their coordinates were set from the uniform distribution and their initial peculiar velocities are equal to zero. The high resolution simulation has 10 times more particles  $N_{total} = 10^6$ . As  $f_{PBH}$  varies from one simulation to another, we adjust the box size accordingly in order to achieve the desired particle density. Therefore, the box size varies from  $15.21 h^{-1}$  kpc for  $f_{PBH} = 1.0$ , to  $706.04 h^{-1}$  kpc for  $f_{PBH} = 10^{-4}$  ( $1521.12 h^{-1}$  kpc for the high resolution simulation).

In order to reduce possible artefacts due to periodicity of the relatively small box, the final redshift of the simulations was set to  $z = 3$ . A total of 200 snapshots were stored at redshift intervals equally-spaced in logarithmic scale, starting from  $z = 10^5$  to  $z = 3$ .

All simulations share the same cosmological parameters in agreement with the values obtained by the Planck Collaboration et al. (2014), i.e.  $\Omega_{\Lambda,0} = 0.692885$ ,  $h = 0.6777$ ,  $\sigma_8 = 0.8288$ ,  $n_s = 0.9611$ . The matter density is taken as  $\Omega_{m,0} = 0.307023$ , while radiation density is taken as  $\Omega_{r,0} = 0.000092$ , where  $\Omega_{m,0} + \Omega_{r,0} = 0.307115$  and, accordingly,  $\Omega_{m,0} + \Omega_{r,0} + \Omega_{\Lambda,0} = 1.0$ .

A summary of the most relevant parameters of the simulations is given in Table 1.

<sup>3</sup> <http://wwwmpa.mpa-garching.mpg.de/~volker/gadget/>

<sup>4</sup> <https://www.bsc.es/>

**Table 1.** Most relevant parameters of the simulation suite.

Fraction $f_{PBH}$	1.0	$10^{-1}$	$10^{-2}$	$10^{-3}$	$10^{-4}$	$10^{-4}$
Box Size ( <i>kpc/h</i> )	15.21	32.77	152.11	327.71	706.04	1521.12
N. particles $N_{total}$	$10^4$	$10^4$	$10^5$	$10^5$	$10^5$	$10^6$
Mass res. ( $M_{\odot}$ )	30	30	30	30	30	30
Grav. soft. $\epsilon$ ( <i>pc</i> )	$10^{-3}$	$10^{-3}$	$10^{-3}$	$10^{-3}$	$10^{-3}$	$10^{-3}$
Min. timestep $\Delta t_{min}$	$10^{-6}$	$10^{-6}$	$10^{-6}$	$10^{-6}$	$10^{-6}$	$10^{-6}$
Initial redshift	$10^5$	$10^5$	$10^5$	$10^5$	$10^5$	$10^5$

### 3 FORMATION AND STABILITY OF PBH PAIRS

In this Section we estimate the PBH pair formation rate and evaluate the possibilities for the pair to be disrupted due to numerical errors rather than to physical processes.

For the analysis of the formation of pairs in our simulations, we calculate the total energy  $E$  of a two body system for every particle and its closest neighbour (see Equation 1). We consider a pair of particles to be gravitationally bound to each other if the condition  $E < 0$  is fulfilled. Naturally, there are certain amount of pairs, which have more than one neighbour that is gravitationally bound to it. This amount varies from 1% to 20% of the total *pairs*, depending on redshift and the fraction of PBH. In the context of the method, which we use for the evaluation of the merger rate (see Section 1), as well as for simplicity, we still treat such pairs as *binaries*, and only account for the neighbour with the minimal total energy value (which could not necessarily be the closest neighbour).

As we mentioned in §1, aside from classical Newtonian captures we also considered the possibility that energy radiated as GW during close hyperbolic encounters might be sufficient to result in binding the given pair, i.e.,  $E - T|E| < 0$ . We found out that even though such events are possible, they are extremely rare and are not present at all for simulations with  $f_{PBH} < 0.1$ . We compared the number of such events,  $n_{cap(GR)}$  (i.e. GR-related capture) with the number of pure Newtonian captures,  $n_{cap(Nt)}$ , to gain some perspective. In Table 2 we quote the ratio of these two number as a function of the PBH fraction of the different simulations. Therefore, we are confident that, at least for our simulation set, the proper accounting of GR corrections to coordinates and velocities is probably not necessary. However, as we already mentioned, this effect is only present in simulations with higher values of  $f_{PBH}$ . But at the same time, these two simulations in our set have the least number of particles ( $N = 10000$ ). Therefore, if we considered a larger simulation with similar values of  $f_{PBH}$  ( $N = 10^6$ , for example), this effect ought to be studied in more detail.

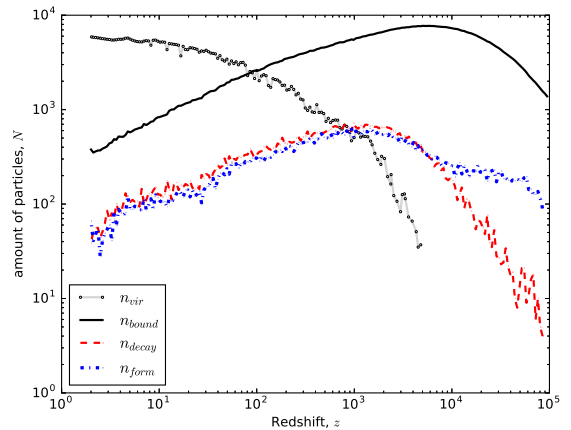
After that, we evaluate the rates of classical bound pairs formation and pair disruption, depending on redshift  $z$  (see Figure 2 for  $f_{PBH} = 1.0$ ).

As one can see from this Figure, the rates of formation and disruption of pairs both grow rapidly towards the radiation-matter equipartition epoch, and then, shortly after, start to decay due to the process of matter virialisation (which we discuss in Section 3.3).

Before going any further, we have to check that this behaviour is not caused by artefacts of the numerical calculation. Therefore, in what follows we study the problem of

**Table 2.** The ratio of the number of GR captures ( $n_{cap(GR)}$ ) to the total number of pure Newtonian captures ( $n_{cap(Nt)}$ ), for the simulations with different PBH fraction ( $f_{PBH}$ )

$f_{PBH}$	$n_{cap(GR)}/n_{cap(Nt)}$
1.0	0.00011
$10^{-1}$	0.00042
$10^{-2}$	0.
$10^{-3}$	0.
$10^{-4}$	0.
$10^{-4}(N_{total} = 10^6)$	0.

**Figure 2.** Number of PBH particles  $n$  as a function of redshift  $z$  for a PBH fraction  $f_{PBH} = 1.0$ , where  $n$  represents various sub-sets of PBH particles (see legend):  $n_{bound}$  – a total amount of gravitationally bound particles in the simulation;  $n_{form}$  – an amount of particles, which are currently (i.e. between two snapshots) forming a pair;  $n_{decay}$  – particles in a pair which is decaying at the given redshift  $z$ . And  $n_{vir}$  represent particles, which are currently part of a virialised structure (see Section 3.3).

pair stability as a function of the softening length, time integration step and multi-particle interactions, including the formation of virialised clusters.

#### 3.1 Softening Length

In most of the modern N-body codes the gravitational potential is *softened* in order to avoid the singularity at small distances between particles, which may result in close-to-zero timesteps and unreasonably long calculation times. In GADGET-2 the single particle density distribution function  $\tilde{\delta}$  is the Dirac  $\delta$ -function convolved with a normalized gravi-

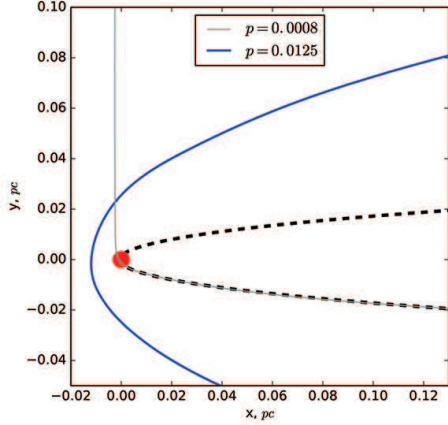


**Figure 3.** Trajectories of particles with various pericentre distances. Blue solid line correspond to the simulated orbit with  $p = 0.0125$  pc and light gray correspond to  $p = 0.0008$  pc. The dashed black line represents the theoretical trajectory for the particle with  $p = 0.0008$  pc. The red solid circle represents the softening length  $\epsilon = 0.001$ .

tational softening kernel of comoving scale  $\epsilon$ . In GADGET-2 the spline kernel (Monaghan & Lattanzio 1985), often used in SPH, is chosen and set to  $\tilde{\delta} = W(|x|, 2.8\epsilon)$ , where  $W(r)$  is given by

$$W(r, h) = \frac{8}{\pi h^3} \begin{cases} 1 - 6(\frac{r}{h})^2 + 6(\frac{r}{h})^3, & 0 \leq \frac{r}{h} \leq \frac{1}{2}, \\ 2(1 - \frac{r}{h})^3, & \frac{1}{2} \leq \frac{r}{h} \leq 1, \\ 0, & \frac{r}{h} > 1 \end{cases} \quad (6)$$

(see Springel (2005))

In the context of our simulations this means, that if two gravitationally bound particles have a very small pericentre distance  $p = a(1 - e)$ , they may get “artificially” disrupted due to the gravitational potential being calculated as  $-Gm/\epsilon$  at such distances, as implied by 6. This might lead to significant numerical errors in the calculated velocities of the particles. This effect is shown in Figure 3 for a particle orbit with  $p = 0.0008$  pc, where the gravitational softening  $\epsilon = 0.001$  pc (exactly as in our main simulation set). On the other hand, a particle with an orbit with  $p = 0.0125$  pc does not get disrupted.

In order to ensure that our choice of softening length  $\epsilon = 0.001$  pc is reasonable, we compare two simulations with different softening lengths  $\epsilon_1 = 0.001$  pc and  $\epsilon_2 = 0.02$  pc, while we keep the PBH fraction  $f_{PBH} = 1.0$  and the other initial parameters. For both simulations we pick up the pairs which are getting disrupted during the given snapshot and evaluate the mean anomaly<sup>5</sup> at the previous snapshot for these pairs. This allows us to trace the moment of pericentre passage for every pair. If at the previous snapshot we notice that the pair is about to pass the pericentre, but at the given snapshot it is disrupted, and moreover, if the pericentre distance for this pair is less than the softening length ( $p < 2.8\epsilon$ ), then we conclude, that the disruption was caused by the softening.

<sup>5</sup> i.e. the fraction of an elliptical orbit’s period that has elapsed since the orbiting body passed its pericenter

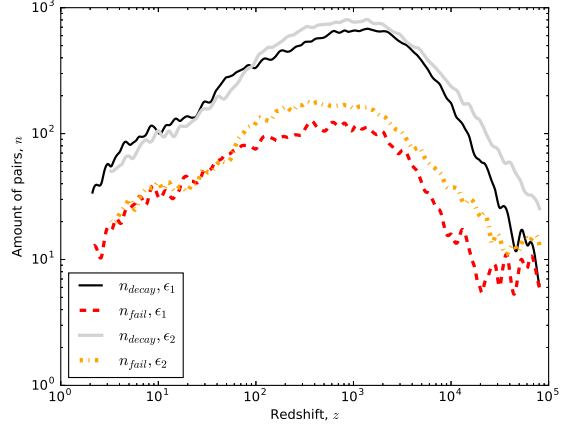


**Figure 4.** Non-solid lines: amount of pairs disrupted due to gravitational softening in both simulations (PBH fraction  $f_{PBH} = 1.0$ ), Solid lines: total amount of pairs disrupted per snapshot in both simulations. Where  $\epsilon_1 = 0.001$  pc and  $\epsilon_2 = 0.02$  pc are the softening lengths in each simulation, accordingly (see legend).

In Figure 4 we display the respective amounts of pairs disrupted due softening of the gravitational potential, and the total amount of disrupted pairs per snapshot for each simulation. As can be seen, the amount of pairs disrupted due to softening (or “artificially”, as we noted above) is relatively small, compared to the total amount of disrupted pairs. In the case of simulation with smaller softening length  $\epsilon_1 = 0.001$  pc the amount of “artificially” disrupted pairs is approximately 20% less than in the case of the simulation with  $\epsilon_2 = 0.02$  pc. However, it is worth noting, that this improvement comes at the cost of 10 - 15 times larger CPU-hours requirements. Therefore, we may conclude that our choice of the gravitational softening length is reasonable and that a further reduction is probably unnecessary.

### 3.2 Time integration numerical errors

In GADGET-2 the “leapfrog” time integration scheme is used which, compared to ordinary numerical integration methods like a high order Runge-Kutta, provides a much better orbital energy conservation and is more stable overall. However, depending on the timestep, the integration errors might still be considerable for a specific problem, which is why we perform a test set of ideal 2-body simulations using the GADGET-2 code. The initial parameters of these simulations are almost exactly the same as for our main simulation set, except that we made an additional simulation with a smaller timestep  $\Delta t = 10^{-7}$  (compared to  $\Delta t = 10^{-6}$  used in our main set). We also turned off the box periodicity and eliminated the Hubble expansion, switching from comoving coordinates to physical ones. Precisely two particles are placed into an otherwise empty cube with initial conditions for coordinates and velocities corresponding to the pair’s eccentricity  $e = 0.9877$  and the orbital period  $T = 0.0123$  Gyr<sup>6</sup>. We have run the simulation for a total

<sup>6</sup> 1 Gyr =  $10^9$  years

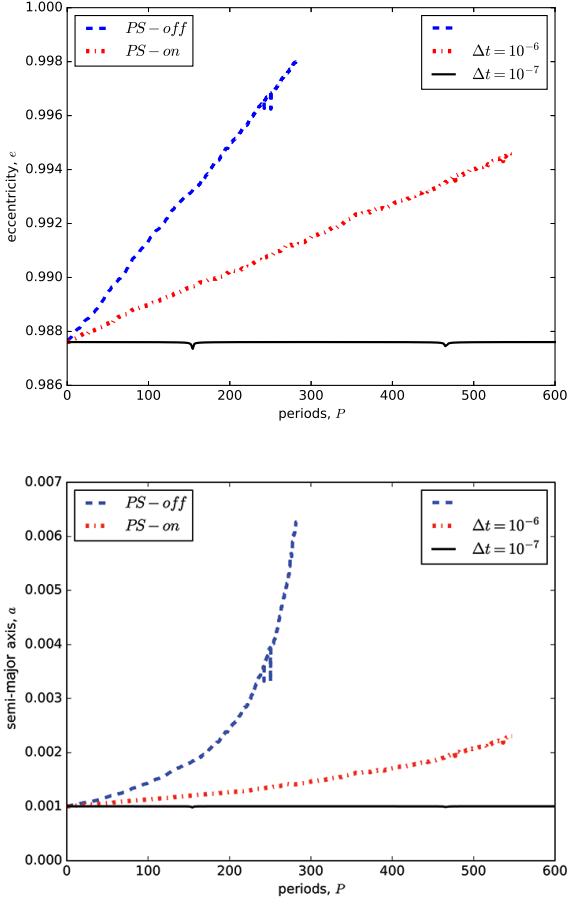


**Figure 5.** Analysis of the orbital change of a two body system dues to numerical time integration errors in GADGET-2. The binary pair eccentricity  $e$  (top panel) and the semi-major axis  $a$  (bottom panel) as a function of time in units of the orbital periods. The *Blue dashed line* corresponds to the simulation with the PSEUDOSYMMETRIC property on and timestep  $\Delta t = 10^{-6}$ , *red dot-dashed line* represents the simulation with PSEUDOSYMMETRIC property off and timestep  $\Delta t = 10^{-6}$ . *Solid black line* represents the simulation with a timestep  $\Delta t = 10^{-7}$ . Results from this simulation are not affected by the PSEUDOSYMMETRIC compile option

time  $t \approx 1000 \times T = 12.5$  Gyr. As it can be seen from Figure 5, for the case with a smaller timestep  $\Delta t = 10^{-7}$  (solid black line) the orbit remains surprisingly stable over the course of the whole simulation. However, for certain simulations in our main set (depending on the PBH fraction  $f_{PBH}$  and the total amount of particles  $N_{total}$ ) such a small timestep value may result in unreasonably long calculation times.

In order to reduce the impact of the numerical errors with higher timestep values we enable the compile flag PSEUDOSYMMETRIC in the GADGET-2 Makefile. When this option is set, the code will try to “anticipate” timestep changes by extrapolating the change of the acceleration into the future. This can in certain idealised cases (such as ours) improve the long-term integration behaviour of periodic orbits (Springel 2005). As one can see from Figure 5, with PSEUDOSYMMETRIC option enabled, the orbital parameters of the pair decay much slowly compared to the case when this option is dis-

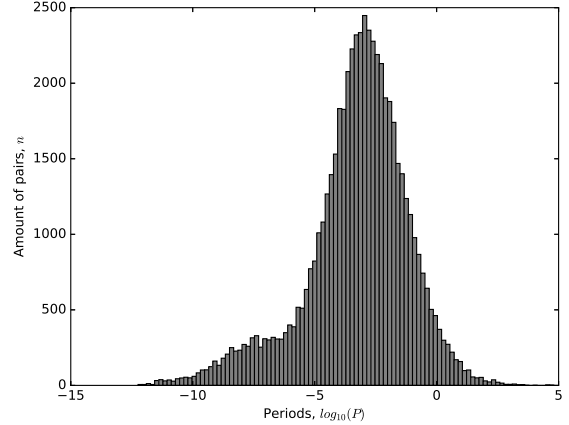


**Figure 6.** The distribution of pair disrupting events throughout the whole simulation as a function ( $f_{PBH} = 1.0$ ) of  $\log_{10}(P)$ , with  $P$  being the number of orbital periods passed before the pair is disrupted. I.e., “0” represents one full period.

abled. In less than 300 periods the value of the semi-major axis for the simulation without PSEUDOSYMMETRIC flag increases by more than  $\sim 500\%$ , compared to only  $\sim 40\%$  for the case with PSEUDOSYMMETRIC flag enabled. However, in the main simulation set, less than 5 pairs per snapshot have survived for even 100 periods before their subsequent disruption, while the absolute majority of pairs tend to disrupt after less than 1 period (see Figure 6). Thus, we conclude that disruption happens due to other reasons rather than numerical errors.

### 3.3 Virialisation of Matter

According to most models of PBH binaries, the mechanism responsible for pair breaking is tidal disruption by nearest neighbours (e.g, see Ali-Haïmoud (2018); Raidal et al. (2019)). In our unperturbed  $\Lambda$ CDM model with Poissonian initial conditions, virialised structures containing many particles start to emerge at redshifts  $z \approx 10^3$ . On the other hand, in classical WIMP DM simulations structures start to form much later, at  $z < 100$  (Ishiyama et al. 2013), and in general, it is worth noting, that normal dark matter haloes would differ significantly from PBH dark matter haloes. In this work we *do not* study the behaviour of PBH pairs in haloes consisting of *normal DM*, as it was mentioned above (see Section 2). As the density inside a newly formed DM halo starts to rise, the distance between particles decreases, naturally, the distance to the nearest neighbour also decreases.

As shown in Figure 2, pairs formation and decay rates start to be damped at  $\approx 10^3$ , while the rate of orbit destabilisation rapidly increases. In order to identify virialised structures formed by PBH particles, we analysed our simulations with the publicly available halo-finding tool AHF<sup>7</sup>, considering a minimum amount of PBH particles per halo  $N_{min} = 10$  and an overdensity parameter  $D_{vir} = 200$ .

In Figure 2, the *grey connected dots* represent the

<sup>7</sup> <http://popia.ft.uam.es/AHF/>

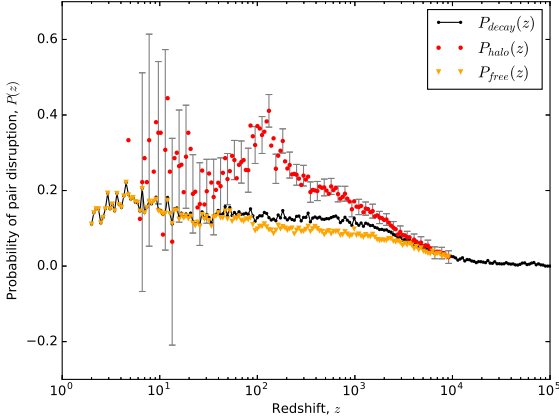


**Figure 7.** Probabilities of pair disruption: inside PBH DM halos  $P_{halo}$  (red dots), outside halos  $P_{free}$  (orange triangles) and the total probability of pair disruption per snapshot  $P_{decay}$  (black solid line) as a function of redshift  $z$ . These results correspond to the simulation with  $f_{PBH} = 1.0$

amount of particles, which are currently part of a PBH-matter halo. Tracking the indices of the particles with the AHF tools allows us to classify all gravitationally *bound* particles  $n_{bound}$  into two sub-sets: particles that are bound inside some of the PBH halo  $n_{halo}$ , and particles that are gravitationally bound to each other, but do not belong to any halo,  $n_{free}$ . Obviously,  $n_{halo} + n_{free} = n_{bound}$ . Since we know the indices of all the gravitationally bound particles, as well those for the disrupted particles, we can now obtain the probabilities of pair disruption inside the PBH halo  $P_{halo}(i)$ , outside the halo  $P_{free}(i)$ , and the total probability  $P_{decay}(i)$  of pair disruption at the a given snapshot  $i$  as follows:

$$P_{halo}(i) = \frac{m_{halo}(i)}{n_{halo}(i-1)}, \quad (7)$$

$$P_{free}(i) = \frac{m_{free}(i)}{n_{free}(i-1)}, \quad (8)$$

$$P_{decay}(i) = \frac{n_{decay}(i)}{n_{bound}(i-1)}, \quad (9)$$

where  $m_{halo}(i)$  and  $m_{free}(i)$  represent the amount of disrupting particles inside and outside of the PBH halo respectively at the  $i$ -th snapshot, and  $m_{halo}(i) + m_{free}(i) = n_{decay}(i)$ , while  $n_{halo}(i-1) + n_{free}(i-1) = n_{bound}(i-1)$  represent the amount of bound particles at  $(i-1)$ -th snapshot.

As one can see from Figure 7, the probability of pair disruption inside PBH halos is significantly higher compared to that one outside halos, as soon as the “*first*” virialised structures begin to emerge between redshifts  $z = 10^4$  and  $z = 10^3$ , which corresponds to radiation-matter equipartition, or even prior that. Large error values at lower redshifts ( $z < 10$ ) are related to extremely small amount of pairs still remaining in halos.

The “*first*” gravitationally-bound structures that we are able to find with AHF halo finder appear to be small clusters of the size of  $\sim 10$  particles (which is the value we

used in AHF to define the minimum number of particles per halo  $N_{min} = 10$ ). Such tiny structures can hardly be considered halos in the traditional meaning. In the case of our simulation set, “*classic*” halos with many particles can be detected only in simulations with larger PBH fraction, such as  $f_{PBH} = 1.0$  and  $f_{PBH} = 0.1$ . In reality, however, gravitationally-bound structures as small as 3-10 particles do exist in all of our 5+1 simulations. Finding such gravitationally-bound structures at high redshifts, in simulations with low values of PBH fraction, using with conventional methods, represents a significant challenge. This seem to happen due to conceptual restrictions of the cosmological halo-finding techniques based on Bound Density Maxima algorithms, which require a measurable level of density contrast for a *reliable* halo detection, while at earlier redshifts the density contrast caused by such a small clusters is virtually non-existent. Attempting to use halo finders based on Friends-Of-Friends (*FOF*) algorithm (see Davis et al. (1985)) does not yield any meaningful results, since for our case the threshold distance can not be chosen unambiguously, as the variations of inter-particle distance both in the field and inside the clusters are large. I.e., the result will depend on the choice of threshold distance.

We conclude that the fraction of virialised matter is actually higher at high redshift,  $z \geq 10^3$ , than is shown in our Figure 2, so we cannot reliably estimate the impact of clusters of PBH particles on pair disruption at that time. At later times,  $z \sim 10^2$ , when virialised PBH matter is condensed in large halos, our estimates of virialisation impact should be correct.

#### 4 PBH MERGERS AND $f_{PBH} < 1.0$

In the previous Section we came to the conclusion that numerical errors do not seem to play any significant role in the process of pair formation and disruption. Instead, it appears that the most significant factor in that process is matter virialisation, that starts happening at  $z \approx 3000$ .

Now we can proceed to our main goal: to estimate the merger rate of PBH pairs from our simulations with different fraction of dark matter in the form of PBHs. The number of gravitationally-bound particles for each simulation is shown in Figure 8. For each *given snapshot* we look for PBH pairs that were formed at the *previous snapshot* and survived (see Section 3). We consider such a pair as a *newly formed* one. Then we calculate the mean anomaly of the pair and observe it gradually changing at each snapshot, during which the pair remains gravitationally bound. If particles pass the pericentre, we calculate the left and right terms of the merge condition (see Eq. 2) at the given snapshot. If the pair is disrupted after passing the pericentre (see Section 3.1) we calculate these two terms of the merger condition using the orbital parameters from the previous snapshot. In this way we do not miss those pairs which were “*unfairly*” disrupted when their particles passed each other within a distance shorter than the softening length. When this condition is satisfied, we declare the pair as “*merged*”. It is also worth noting that for PBH of masses  $M = 30M_{\odot}$ , the maximum possible pericentre for the merging pair is  $2.6 \times 10^{-4}$  pc, which can be calculated assuming the merger time for the pair to be less than  $\sim 10$  Gyr. In practice, however, af-

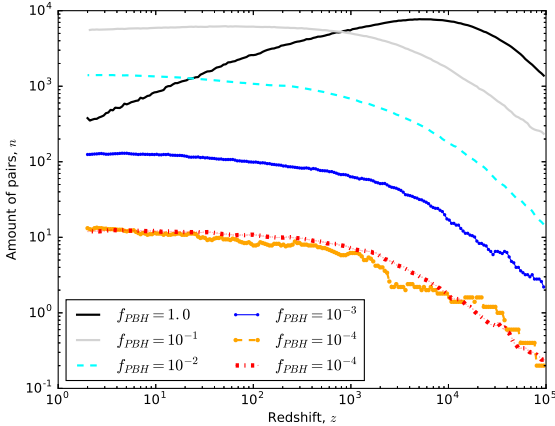


**Figure 8.** Number of PBH pairs that remain *gravitationally-bound* during the entire simulation as a function of redshift. The total number of particles is fixed to  $N = 10^4$ . Simulations with  $N > 10^4$  are rescaled to that value. The different lines correspond to simulations with different fractions of dark matter in the form of PBHs, varying from  $f_{PBH} = 1.0$  to  $f_{PBH} = 10^{-4}$  (see legend for specific symbols). The *orange dashed line* represents the simulation with  $f_{PBH} = 10^{-4}$  and the total number of particles  $N = 10^5$ , while *red dot-dashed line* represents the simulation with the same PBH fraction but for  $N = 10^6$ .

ter merging the particles still remain where they are and the pair, in fact, does not get replaced by twice a heavier particle. Since the amount of pairs should decrease after merging, in order to avoid over-abundance of acting particles in the simulation we artificially “delete” one of the particles from the merged pair. So that when such pair is disrupted, only one of the particles is now considered as “free”, and another one is ignored for the rest of the simulation. We have also checked that our results on the merger rate do not change significantly if we keep both particles of a merged pair, or if we delete both of them.

In Figure 9 we show the corresponding merger rates,  $r_m$  for each of our simulations listed in Table 1. As can be seen in that Figure, we fail to detect merger events below a certain redshift, for all the five simulations. Therefore, we decided to make an additional simulation (described in Section 2) with an increased number of PBH particles  $N = 10^6$  in order to verify how the particle number would improve this situation. The *orange-bordered white hexagons* in Figure 9 represent this high resolution simulation, with 10 times more particles (compared to the main simulation set with  $f_{PBH} = 10^{-4}$  and  $N = 10^5$  particles) one can observe significantly more merger events, while the merger rate per  $\text{Gpc}^3$  per year for the PBH fraction remains approximately the same. Additionally, as we mentioned in §1, we also considered mergers caused by GW radiation in close hyperbolic encounters, and it appeared that only 0.77% of all mergers throughout all our 6 simulations had hyperbolic orbits, and only the simulations with the higher fraction of PBH (1.0 and 0.1) had just a measurable number of such mergers (see Table 2).

In order to register merger events at  $z = 3$  for a PBH fraction  $f_{PBH} = 10^{-3}$  we would have to increase the amount of particles in the simulation from  $N = 10^5$  to approxi-

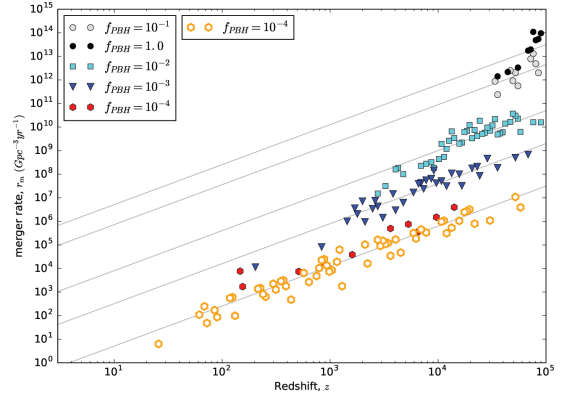


**Figure 9.** The merger rate of PBH binaries,  $r_m$ , as a function of redshift  $z$  (see legend for specific symbols). *Red filled hexagons* represent the results for the simulation with  $f_{PBH} = 10^{-4}$  and  $N = 10^5$  particles, while *orange-bordered white hexagons* represent the high resolution simulation with  $f_{PBH} = 10^{-4}$  and  $N = 10^6$  particles. The extrapolated values to the corresponding points for different PBH fractions are represented by *light-gray straight lines*

mately  $N = 10^8$ , which would increase the computational time by an order of 100 to 1000, resulting in a simulation of  $> 10^6 - 10^7$  of CPU-hours. As an alternative, we can just simply extrapolate our result to the given redshift. The results of this extrapolation are shown in Figure 9 as *light-gray straight lines*. In the case with  $f_{PBH} = 10^{-3}$ , the merger rate roughly corresponds to  $r_m \approx 10^2 \text{ Gpc}^{-3} \text{ yr}^{-1}$  at redshift  $z \approx 3$ . However, despite the fact that the result for this PBH fraction matches the estimation of the merger rate by the LIGO collaboration (Abbott et al. 2016c) and by other groups (Ali-Haïmoud 2018; Raidal et al. 2019), such an extrapolation might not be well suited for the estimation of the merger rates for PBH fractions  $f_{PBH} > 0.001$  and it merely represents a qualitative result here. As we discussed in Section 3.3, the formation of large gravitationally-bound structures (such as DM halos) might prevent merger events from occurring altogether, while on the other hand, a choice of a more realistic model (for example, the one with the proper account of GR effects in dense clusters, as discussed in a recent paper by Trashorras et al. (2020)) may complicate things even further.

## 5 CONCLUSIONS

The main purpose of this work is to expand our understanding of the process of formation, disruption and merging of bound and unbound pairs of primordial black holes (PBHs) as one of the possible candidates responsible for the events registered by The Advanced Laser Interferometer Gravitational-Wave Observatory (LIGO), including Abbott et al. (2016a,b,c, 2017a,b,c).

We performed a series of cosmological simulations in a box with periodic boundary conditions, where either all of the dark matter or a variable fraction  $f_{PBH}$  is represented by primordial black holes (PBHs) with  $30 M_\odot$  masses. We assume that “normal” dark matter constitute an homogeneous



fluid with no density fluctuations, that only contributes to the evaluation of Hubble function. We showed that this assumption is reasonable for  $z \geq 10$ . However, we have pushed our simulations down in redshift, up to  $z = 3$ , at the cost of accuracy. Nevertheless, errors associated to box periodicity would not allow us to run the simulations down to redshift  $z = 0.0$ .

In order to account for the radiation dominated stage of the Universe expansion we use a modified version of public N-body code **GADGET-2** (Springel 2005) with specific parameters tuned to calculate the orbital parameters of the forming PBH pairs with sufficient precision to accurately track their orbits until they merge or get disrupted by interactions with their neighbours. Additionally, we concluded that the number of binary captures during hyperbolic close encounters due to GR effects is negligible compared to the number of pure Newtonian captures.

We devote a significant amount of effort in order to verify that the measured pair disruption is not caused by the intrinsic numerical errors associated to any N-body computation of gravitational orbits (see Figure 2 and Section 3.2). As a result, we ensured, that this is not the case, and that the main factor responsible for the processes of PBH pairs formation, disruption and merging is the emerging of gravitationally bound structures around redshifts of  $z \approx 3000$ , which roughly corresponds to the radiation-matter equipartition epoch.

We have also reported our findings on the merger rates of PBH pairs, including hyperbolic mergers, which represent 0.77% of the total number of mergers across all 6 simulations. By comparing the merger rates of simulations with the same PBH fraction  $f_{PBH} = 10^{-4}$  and varying amount of particles,  $N = 10^5$  and  $N = 10^6$ , we demonstrated that the sample size affects the amount of registered merger events but, at the same time, the merger rate remains approximately the same. Then we extrapolate the merger rate trends for all PBH fractions up to the redshift  $z = 3$ , where we estimate a merger rate value of  $r_m \approx 10^2 Gpc^{-3} yr^{-1}$  for PBH fraction of  $f_{PBH} = 10^{-3}$ , which nicely matches the merger rate estimated by the LIGO collaboration (Abbott et al. 2016c) and other groups (Ali-Haïmoud 2018; Raidal et al. 2019).

However, our estimations of the merger rates for larger values of PBH fractions ( $f_{PBH} > 0.01$ ) might be significantly overestimated, because the simple extrapolation does not account for the influence of the processes related to matter virialisation. On the other hand, as it has been recently shown by Luca et al. (2020), accretion processes existing prior to redshift  $z \sim 10$  might also affect the PBH abundance. As discussed by these authors, the accretion rate depends significantly on the relative velocity between the PBHs and baryonic matter. Therefore, virialisation might play even a more important role in the evolution of PBH pairs than we have suggested in Sec. 3.3.

In this paper we have discussed the qualitative implementations of this phenomena – but, obviously, a more thorough quantitative analysis is required. Therefore, in a future work we plan to create new numerical simulations, where the “normal” DM would be represented as a separate type of N-body particles with their corresponding initial conditions compatible with the  $\Lambda$ CDM cosmological model.

## ACKNOWLEDGEMENTS

We are eternally indebted to P. B. Ivanov for many illuminating discussions and comments. The work of MVT and SVP was supported by RFBR grant 19-02-00199. GY acknowledges financial support from *Ministerio de Ciencia, Innovación y Universidades / Fondo Europeo de Desarrollo Regional*, under research grant PGC2018-094975-C21. We would like to thank the *Red Española de Supercomputación* for granting us access to the MARENOSTRUM supercomputer at the BSC-CNS where the simulations used in this work have been run.

## DATA AVAILABILITY

The data underlying this article will be shared on reasonable request to the corresponding author.

## REFERENCES

- Abbott B. P., et al., 2016a, *Phys. Rev. Lett.*, **116**, 061102  
 Abbott B. P., et al., 2016b, *Phys. Rev. Lett.*, **116**, 241103  
 Abbott B. P., et al., 2016c, *ApJ*, **818**, L22  
 Abbott B. P., et al., 2017a, *Phys. Rev. Lett.*, **118**, 221101  
 Abbott B. P., et al., 2017b, *Phys. Rev. Lett.*, **119**, 141101  
 Abbott B. P., et al., 2017c, *ApJ*, **851**, L35  
 Ali-Haïmoud Y., 2018, *Phys. Rev. Lett.*, **121**, 081304  
 Carr B., Kühnel F., Sandstad M., 2016, *Phys. Rev. D*, **94**, 083504  
 Carr B., Raidal M., Tenkanen T., Vaskonen V., Veermäe H., 2017, *Phys. Rev. D*, **96**, 023514  
 Clesse S., García-Bellido J., 2018, *Physics of the Dark Universe*, **22**, 137  
 Clesse S., García-Bellido J., 2017, *Physics of the Dark Universe*, **15**, 142–147  
 Davis M., Efstathiou G., Frenk C. S., White S. D. M., 1985, *ApJ*, **292**, 371  
 Dolgov A. D., 2017, in *European Physical Journal Web of Conferences*. p. 01012 ([arXiv:1701.05774](https://arxiv.org/abs/1701.05774)), [doi:10.1051/epjconf/201714201012](https://doi.org/10.1051/epjconf/201714201012)  
 Espinosa J. R., Racco D., Riotto A., 2018, *Phys. Rev. Lett.*, **120**, 121301  
 Garcia-Bellido J., Clesse S., Fleury P., 2017, LIGO Lo(g)Normal MACHO: Primordial Black Holes survive SN lensing constraints ([arXiv:1712.06574](https://arxiv.org/abs/1712.06574))  
 García-Bellido J., Nesseris S., 2017, *Physics of the Dark Universe*, **18**, 123–126  
 Inman D., Ali-Haïmoud Y., 2019, *Physical Review D*, **100**  
 Ishiyama T., et al., 2013, *ApJ*, **767**, L46  
 Kashlinsky A., 2016, *The Astrophysical Journal*, **823**, L25  
 Lacki B. C., Beacom J. F., 2010, *The Astrophysical Journal*, **720**, L67  
 Luca V. D., Franciolini G., Pani P., Riotto A., 2020, Primordial Black Holes Confront LIGO/Virgo data: Current situation ([arXiv:2005.05641](https://arxiv.org/abs/2005.05641))  
 Monaghan J. J., Lattanzio J. C., 1985, *A&A*, **149**, 135  
 Nakamura T., Sasaki M., Tanaka T., Thorne K. S., 1997, *ApJ*, **487**, L139  
 Nitz A. H., Capano C., Nielsen A. B., Reyes S., White R., Brown D. A., Krishnan B., 2019, *The Astrophysical Journal*, **872**, 195  
 Peters P. C., Mathews J., 1963, *Phys. Rev.*, **131**, 435  
 Planck Collaboration et al., 2014, *A&A*, **571**, A16  
 Press W. H., Schechter P., 1974, *ApJ*, **187**, 425  
 Raidal M., Vaskonen V., Veermäe H., 2017, *Journal of Cosmology and Astro-Particle Physics*, **2017**, 037

- Raidal M., Spethmann C., Vaskonen V., Veermäe H., 2019, [Journal of Cosmology and Astro-Particle Physics](#), **2019**, 018
- Sasaki M., Suyama T., Tanaka T., Yokoyama S., 2016, [Phys. Rev. Lett.](#), **117**, 061101
- Sasaki M., Suyama T., Tanaka T., Yokoyama S., 2018, [Classical and Quantum Gravity](#), **35**, 063001
- Springel V., 2005, [MNRAS](#), **364**, 1105
- The LIGO Scientific Collaboration et al., 2018, arXiv e-prints, p. [arXiv:1811.12907](#)
- Trashorras M., García-Bellido J., Nesseris S., 2020, The clustering dynamics of primordial black holes in  $N$ -body simulations ([arXiv:2006.15018](#))
- Turner M., 1977, [ApJ](#), **216**, 610
- Wang S., Wang Y.-F., Huang Q.-G., Li T. G. F., 2016, arXiv e-prints, p. [arXiv:1610.08725](#)
- Zel'dovich Y. B., Novikov I. D., 1966, [Azh](#), **43**, 758
- Zumalacárregui M., Seljak U. c. v., 2018, [Phys. Rev. Lett.](#), **121**, 141101

This paper has been typeset from a  $\text{\TeX}/\text{\LaTeX}$  file prepared by the author.